Aurivillius halide perovskite: a new family of two-dimensional materials for optoelectronic applications

Shuai Zhao[a,*], Chunfeng Lan[b], Huanhuan Li[a], Chu Zhang[c], Tingli Ma[c,d]

[a]Chongqing Key Laboratory of Green Energy Materials Technology and Systems, School of Science, Chongqing University of Technology, Chongqing 400054, P.R. China

[b]School of Automotive and Transportation Engineering, Shenzhen Polytechnic, Shenzhen 518055, P.R. China

[c]Department of Materials Science and Engineering, China Jiliang University, Hangzhou 310018, P. R. China

[d]Graduate School of Life Science and Systems Engineering, Kyushu Institute of Technology, Kitakyushu, Fukuoka 808-0196, Japan

[*]E-mail: zhaoshuai@cqut.edu.cn

Abstract

Layered perovskites have attracted considerable attention in optoelectronic applications due to their excellent electronic properties and stability. In this work, the quasi-2D aurivillius halide perovskites are investigated using density functional theory. The single-layer aurivillius perovskite Ba_2PbI_6 is predicted to have a direct bandgap of 1.89 eV, which is close to that of the Ruddlesden–Popper perovskite Cs_2PbI_4. The electronic structures near the Fermi level are mainly governed by the [PbX_6] octahedra, which leads to similar electronic properties to that of Cs_2PbI_4. Decomposition energies reveal that these aurivillius perovskites exhibit thermal instability. Increasing the number of [PbX_6] octahedra layer can enhance the stability and reduce the bandgap. Bi- and In-based aurivillius perovskites are also calculated to evaluate the Pb-free alternatives. These calculations can serve as a theoretical support in exploring novel layered perovskites.

Introduction

Since the first report of organic–inorganic halide perovskite (OIHP) solar cells in 2009, the power conversion efficiency (PCE) has dramatically increased to 25.02%.[1–3] OIHP exhibits unprecedented optoelectronic properties, such as high carrier mobility, large optical absorption coefficient, and low-cost fabrication method.[4–6] Thus, they are promising absorber materials of next-generation solar cells. Apart from photovoltaics, OIHP materials have also been applied in various optoelectronic devices, such as photodetectors and light-emitting diodes.[7] The impressive performance of devices is mainly gained by applying the hybrid perovskites. Therefore, long-term instability must be further improved.

2D layered OIHPs are recently proposed and show better moisture tolerance than their 3D analogues.[8] 2D perovskites consist of large cations and separated perovskite-like sheets. For the perovskite-like sheets, octahedra are connected by the corner-sharing anions. Meanwhile, the large cations are sandwiched between them and provide van der Waals forces to stack the perovskite-like slabs.[9,10] 2D OIHPs possess high quantum efficiency, intense photoluminescence, and excellent flexibility because of their unique layered structure.[11] The dimensional reduction breaks the symmetry of perovskite structure, which affects some optoelectronic properties (e.g., bandgap and exciton binding energy). Previous literature has demonstrated that the thickness of perovskite-like sheets plays a crucial role in controlling the bandgap of 2D OIHP materials, and a PCE of 15.3% has been obtained with 2D perovskite solar cells containing $(PEA)_2(MA)_{59}Pb_{60}I_{181}$ (PEA = $C_6H_5(CH_2)_2NH_3^+$; MA = $CH_3NH_3^+$).[12]

Layered perovskites can be divided into various types according to the structural feature of separated perovskite-like sheets. The mostly used 2D halide perovskites in solar cells commonly belong to the Dion–Jacobson (DJ) or Ruddlesden–Popper (RP) phases. They can be conceptually obtained by cutting the octahedra planes of 3D perovskite ABX_3 along the <100> direction, and the distinction between RP and DJ structures is the number of A-site cation layers. For the RP phase, only the B-X planes are cut off from the 3D structure, and the A-site cations on both sides of the B-X

planes are retained. The chemical formula for this phase is $A'_2{\cdot}A_{n-1}B_nX_{3n+1}$. By contrast, the DJ phase perovskites lose one B-X plane and one adjacent A-site cations plane simultaneously. The chemical formula for this phase is $A'{\cdot}A_{n-1}B_nX_{3n+1}$. Aurivillius perovskite is another layered perovskite structure that can be regarded as cutting B-X planes along the <100> direction of 3D perovskite. In this structure, excessive X-site anions are inserted into the intercalation of adjacent perovskite-like slabs of RP phase perovskites.[13,14] The general formula is $A'_2X_2{\cdot}A_{n-1}B_nX_{3n+1}$. To the best of our knowledge, experiments and calculations are unavailable for aurivillius halide perovskites. In this work, we report theoretical investigations on a series of inorganic aurivillius halide perovskites $Ba_2Cs_{n-1}Pb_nX_{3n+3}$ (n = 1 and 2) by using density functional theory. The optoelectronic properties of these aurivillius compounds are evaluated, which can serve as a useful guide to explore layered perovskites for optoelectronic applications.

Computational methods

All calculations were performed using the Quantum ESPRESSO package based on the plane-wave pseudopotential approach.[15–17] Ultrasoft pseudopotentials were used to describe the interaction between core and valence electrons with the generalized-gradient approximation of Perdew–Burke–Ernzerhof (PBE).[18] The wave functions and charge density were expanded in the plane-wave basis with a kinetic energy cutoff of 40 and 320 Ry, respectively. A 6×6×2 Monkhorst–Pack *k*-mesh grid was used to integrate the Brillouin zone for the unit cell of n = 1 structure and a 6×6×1 *k*-mesh grid was used for the n = 2 and n = 3 structures.[19] The lattice parameters, including the lattice constant and atomic position, were fully relaxed for all 2D layered perovskite structures by using the Broyden–Fletcher–Goldfarb–Shanno algorithm with a force convergence threshold of 10^{-3} Ry/bohr and an energy convergence of 10^{-4} Ry. The optical absorption coefficient $\alpha(\omega)$ was calculated according to the following relation:

$$\alpha(\omega)=\sqrt{2}\,\omega\left[\sqrt{\varepsilon_1^2(\omega)+\varepsilon_2^2(\omega)}-\varepsilon_1(\omega)\right]^{1/2} \quad , \qquad (1)$$

where $\varepsilon_1(\omega)$ and $\varepsilon_2(\omega)$ are the real and imaginary parts of frequency-dependent complex dielectric function, respectively.

Results and discussion

We first investigated the halide aurivillius perovskites $Ba_2Cs_{n-1}Pb_nX_{3n+1}$ (n = 1, 2), where n is the layer number of perovskite-like sheets. For the n = 1 structure, the crystal consists of Ba_2X_2 layers and corner-sharing [PbX_6] octahedra layers with a chemical formula Ba_2PbX_6 (**Figure 1a**). For n ≥ 2, Cs cations occupy the center of tetradecahedron formed by the perovskite-like sheets (**Figure 1b**). With the increase in the number of [PbX_6] octahedra layer to infinity, the aurivillius phase will be equivalent to the 3D analogue $CsPbX_3$. The lattice parameters of aurivillius perovskites Ba_2PbI_6 and $Ba_2CsPb_2I_9$ were optimized by the PBE method, as presented in **Table 1**. The calculated lattice constant *a* of Ba_2PbI_6 is 6.4 Å, which is slightly larger than the predicted value of 6.38 Å for $CsPbI_3$. Given that the ionic radius of Ba is smaller than that of Cs, the elongation of lattice constants that are parallel to the [PbI_6] octahedra layers can be ascribed to the Ba-I interaction. Moreover, the lattice constant *c* of aurivillius Ba_2PbI_6 is longer than that of the RP perovskite Cs_2PbI_4 as a result of an excessive I^- layer between the perovskite-like slabs. Notably, the PbI_6 octahedra in Ba_2PbI_6 and Cs_2PbI_4 exhibit different features. The Pb-I bonds parallel to the octahedra planes are shorter than that along the *c*-axis in Cs_2PbI_4. For the aurivillius Ba_2PbI_6, the Pb-I bond length along the *a*-direction is longer than that of *c*-direction. For $Ba_2CsPb_2I_9$, the Pb-I bond length along the *a*-axis is equal to that of 3D perovskite $CsPbI_3$, which results in the same lattice constant compared with the $CsPbI_3$. The bond length of Pb-I adjacent to the Cs cations is evidently longer than that adjacent to the Ba cations along the *c*-direction due to the large ionic radius of Cs cations.

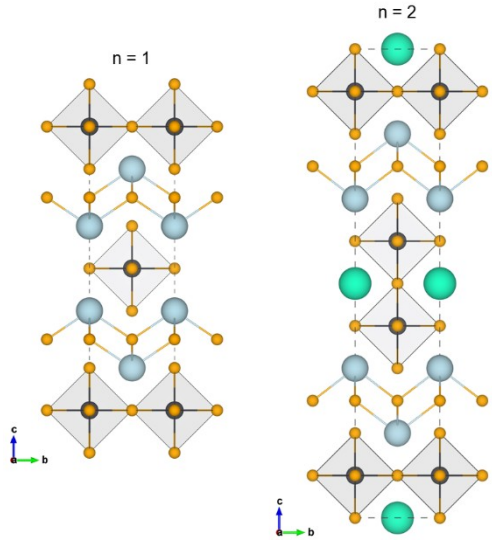

Figure 1. Illustration of aurivillius perovskites (a) Ba_2PbI_6 and (b) $Ba_2CsPb_2I_9$ as viewed along the *a*-axis. Cs, Ba, Pb, and X ions are denoted as green, blue, black, and orange, respectively.

Table 1. Optimized lattice parameters for aurivillius perovskites Ba_2PbI_6 and $Ba_2CsPb_2I_9$ compared with 3D perovskite $CsPbI_3$ and RP perovskite Cs_2PbI_4.

	a (Å)	*c* (Å)	r_{Pb-I} (Å)	r_{Ba-I} (Å)
Ba_2PbI_6	6.40	21.51	3.20 (∥), 3.16 (⊥)	3.53
$Ba_2CsPb_2I_9$	6.38	34.35	3.19 (∥), 3.14 (⊥, outer), 3.21 (⊥, inner)	3.54
Cs_2PbI_4	6.36	19.57	3.18 (∥), 3.23 (⊥)	-
$CsPbI_3$	6.38	6.38	3.19	-

In accordance with the optimized crystal lattice of the aurivillius perovskite Ba_2PbI_6, we calculated the electronic band structure by the PBE method, as depicted in **Figure 2**. The Ba_2PbI_6 exhibits a direct bandgap of 1.89 eV at the S-point in the Brillouin zone. This value is considerably larger than that of 3D $CsPbI_3$ (1.48 eV) and close to that of RP Cs_2PbI_4 (1.90 eV).[20,21] The valence band maximum (VBM) is predominantly composed of antibonding states of Pb 6s and I 5p orbitals, while the

conduction band minimum (CBM) consists mainly of Pb 6p orbitals. The charge density plots further demonstrate that the Ba-I layers have not an obviously influence on the VBM and CBM, and the contribution is mainly from the interaction between the Pb and I in the [PbI_6] octahedra. Therefore, aurivillius Ba_2PbI_6 shows the similar feature of VBM and CBM to RP Cs_2PbI_4. The optical absorption coefficient α of Ba_2PbI_6 shows an anisotropic character along two different directions that are parallel and perpendicular to the [PbI_6] octahedra layers, which indicates that the 2D electronic dimensionality of aurivillius Ba_2PbI_6.[22] Given the 2D layered structure, α along the in-plane direction is stronger than that in out-of-plane direction for low-energy photons. However, Ba_2PbI_6 exhibits the p-p transition feature similar to the 3D $CsPbI_3$, which leads to high absorption coefficient. In Pb halide perovskites, the effect of spin–orbit coupling (SOC) is significant to the band structure.[23] The band structure of Ba_2PbI_6 calculated with PBE+SOC method is shown in **Figure S1**. The low conduction bands undergo a dramatic splitting due to the SOC effect, which leads to an underestimated direct bandgap of 1.01 eV.

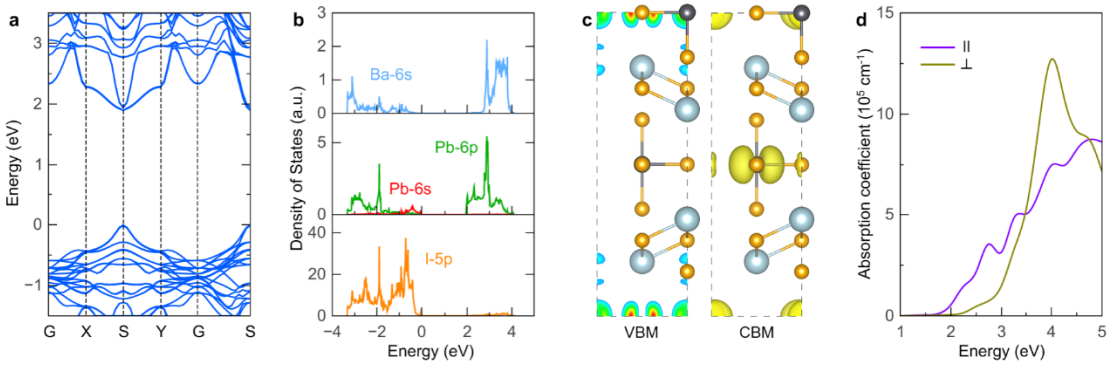

Figure 2. Calculated (a) band structures, (b) PDOS, (c) charge density at the VBM and CBM, and (d) optical adsorption coefficient α along two directions that are parallel or perpendicular to the octahedra layers for aurivillius perovskite Ba_2PbI_6. The top of the valence bands is set to 0 eV.

The absorber materials of solar cells should have a direct bandgap in the range of 1.1–1.6 eV to obtain high efficiency.[24] Layered halide perovskites usually have larger bandgap than their 3D analogues. A feasible method for decreasing the

bandgap of layered perovskites is to increase the layer numbers n. Previous theoretical studies on RP perovskites $Cs_{n+1}Pb_nI_{3n+1}$ have demonstrated that the bandgaps decrease from 1.90 eV with n = 1 to 1.51 eV with n = 10, which is close to 1.48 eV of 3D $CsPbI_3$ corresponding to n = ∞.[22] For these aurivillius perovskites, the bandgap shows a similar trend with the increase in the layer numbers. Moreover, the electronic properties of these aurivillius halide perovskites are mainly determined by the bond character of [PbX_6] octahedra. These aurivillius halide perovskites have a diminishing tendency of bandgaps in order of Cl, Br, and I, as presented in **Table 2**. Thus, the substitution of I by Br or Cl in these aurivillius perovskites could further tune their bandgaps, which suggests their potential application in other optoelectronic fields, such as photocatalytic.

The stability of matter is an important concern for perovskite absorbers. We calculated the decomposition energy (ΔH_d) to evaluate the chemical stability of the aurivillius perovskite $Ba_2Cs_{n-1}Pb_nX_{3n+3}$.[25,26] The decomposition energy was defined via the free energy difference of the decomposition reaction into binary compounds, that is, $\Delta H_d = 2\cdot E(BaI_2) + (n-1)\cdot E(CsI) + n\cdot E(PbI_2) - E(Ba_2Cs_{n-1}Pb_nX_{3n+3})$. Unfortunately, the calculated ΔH_d of these aurivillius perovskites are all negative for n = 1 and 2, which indicates that the decomposition will be spontaneous exothermic reaction. However, the stability can be improved by increasing the layer number of perovskite-like sheets, which is also beneficial to the bandgap optimization.

Table 2. Predicted bandgaps E_g and decomposition energies ΔH_d for aurivillius perovskite $Ba_2Cs_{n-1}Pb_nX_{3n+3}$ (n = 1 and 2) by the PBE method.

	E_g (eV)		ΔH_d (eV/formula)	
	n=1	n=2	n=1	n=2
Cl	2.68	2.53	-0.68	-0.48
Br	2.27	2.08	-0.72	-0.57
I	1.89	1.70	-0.77	-0.69

The environmental risk of toxic Pb leakage is an inescapable concern of the large-scale commercialization of OIHP solar cells. Exploring efficient Pb-free

analogues has been a major challenge for present OIHP investigations.[27] We examined the substitution of Pb with Ge and Sn in the single-layer aurivillius perovskite. The small direct bandgaps are predicted to be 0.85 and 0.82 eV for Ba_2GeI_6 and Ba_2SnI_6, respectively. The high energy levels of Ge 4s and Sn 5s orbitals result in smaller bandgaps for Ba_2GeI_6 and Ba_2SnI_6 than that for Pb-based counterparts. This finding suggests that B-site cation mixture (e.g., Pb/Sn or Pb/Ge) will be another feasible strategy to tune the bandgaps of aurivillius perovskites.

Given that Sn^{2+} cations suffer from the oxidation to +4 state, Sn^{4+}-based vacancy-ordered double perovskite $Cs_2\square SnI_6$ has attracted great interest in optoelectronic applications.[28] Apart from the group IVA elements Ge and Sn, Bi is also a promising alternative of Pb due to the same electronic configuration, $5d^{10}6s^26p^0$, for their stable cations.[29–31] Given the chemical formula $A'_2X_2{\cdot}A_{n-1}B_nX_{3n+1}$, A'-, A- and B-sites should be bivalent, monovalent, and bivalent cations, respectively, to satisfy the total charge neutrality of aurivillius halide perovskites. Otherwise, non-bivalent B-site cations can only probably exist in some certain aurivillius structures. For example, tetravalent B-site cations can only form the single-layer aurivillius halide perovskites with A' = monovalent cations, such as $Cs_2B^{4+}I_6$. However, the trivalent cations can only form the double-layer aurivillius compounds with A' and A = monovalent cations, such as $Cs_3B^{3+}{}_2I_9$. We calculated the electronic structures of $Cs_2B^{4+}I_6$ (B = Ti and Sn) and $Cs_3B^{3+}{}_2I_9$ (B = In and Bi), as shown in **Figure S3**. Although these B-site cations have diverse electronic properties ($3d^04s^0$ for Ti^{4+}, $5s^05p^0$ for In^{3+} and Sn^{4+}, and $6s^26p^0$ for Bi^{3+}), these compounds are computed to be metallic. Notably, these compounds can form other perovskite phases, including vacancy-ordered double perovskite structures for Cs_2TiI_6 and Cs_2SnI_6 (*Fm*3*m*) and 2D or 0D perovskite structures for $Cs_3Bi_2I_9$ (*P*6$_3$/*mmc* and *P*3*m*1).[30,32–35] Comparison of the total energies of different structures shows that the aurivillius structures have the highest energy in each case, which indicates their inferior stability.

In 3D perovskite structure, Pb can be replaced by trivalent Bi by incorporating monovalent cations with 1:1 ratio to form B-site double perovskites, such as

$Cs_2AgInCl_6$ and Cs_2AgBiX_6 (X = Cl and Br). Interestingly, Ag/Bi iodide perovskites can also crystalize in the 2D RP structure, though they have been demonstrated to exhibit thermodynamic instability in the 3D perovskite structure.[36,37] Here, we investigated the electronic structures of aurivillius double perovskites (A-site-ordered and B-site-ordered) by the PBE method, as shown in **Figure 3**. The Bi 6s orbitals form the antibonding state with I 5p orbitals at the VBM, while the In 5s orbitals compose the bonding states with I 5p orbitals at the CBM. However, the two A-site-ordered perovskites exhibit the direct bandgap at the Γ-point. For the B-site-ordered compounds, these perovskites have indirect bandgap due to the effect of Ag 4d orbitals at the VBM.

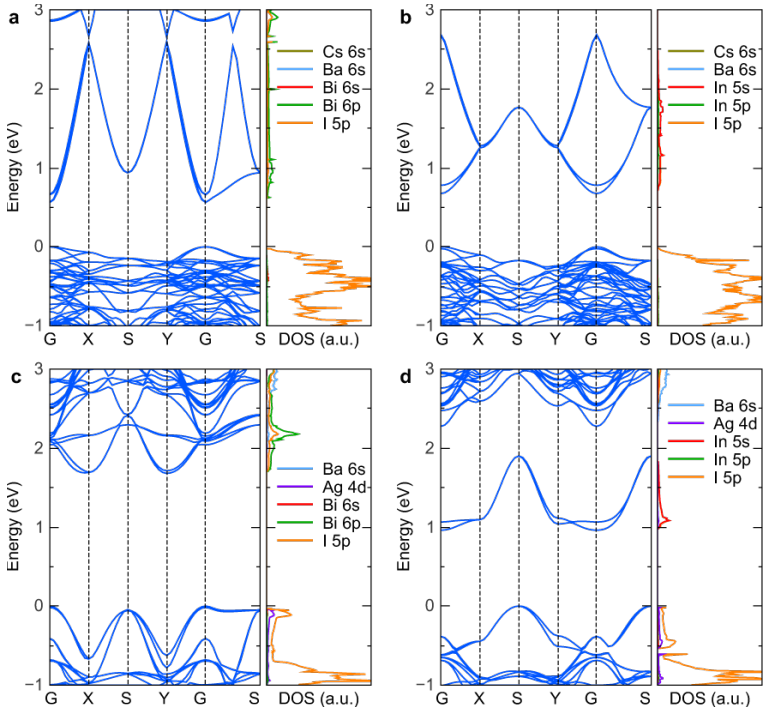

Figure 3. Calculated band structures for Pb-free aurivillius double perovskites. A-site double perovskites (a) $CsBaBiI_6$ and (b) $CsBaInI_6$ and B-site double perovskites (c) $Ba_2Ag_{0.5}Bi_{0.5}I_6$ and (d) $Ba_2Ag_{0.5}Bi_{0.5}I_6$. The top of the valence band is set to 0 eV in each case.

Conclusions

We investigate the electronic properties of a series of inorganic layered aurivillius halide perovskites $Ba_2Cs_{n-1}B_nX_{3n+3}$ by using density functional theory. The Pb-based

aurivillius perovskites show that the direct bandgap and the gap value decrease with the increase in octahedra layers. The bandgap of single-layer Ba_2PbI_6 is predicted to be 1.89 eV, which is close to the single-layer RP perovskite Cs_2PbI_4. This gap value can be further tuned by substituting the X-site anions or B-site cations to meet the requirement of photocatalytic or photovoltaic applications. Moreover, Pb-free aurivillius double perovskites are investigated. Similar to the 3D structure, B^{3+}/B^{+} mixed double perovskites usually have indirect bandgap, while the A-site double perovskites based on Bi^{3+} or In^{3+} exhibit the direct bandgap. Thus, they show promising potential in optoelectronic applications.

Conflicts of interest

There are no conflicts of interest to declare.

Acknowledgements

This work was supported by the National Natural Science Foundation of China (61904114), Post-doctoral Later-stage Foundation Project of Shenzhen Polytechnic (6019211004K), Shenzhen Science & Technology Project (JCYJ20170818092745839), and scientific research start-up fund of Chongqing University of Technology (2017ZD51). This work was carried out at LvLiang Cloud Computing Center of China, and calculations were performed on TianHe-2.

References

(1) Kojima, A.; Teshima, K.; Shirai, Y.; Miyasaka, T. Organometal Halide Perovskites as Visible-Light Sensitizers for Photovoltaic Cells. *J. Am. Chem. Soc.* **2009**, *131* (17), 6050–6051.

(2) Liu, M.; Johnston, M. B.; Snaith, H. J. Efficient Planar Heterojunction Perovskite Solar Cells by Vapour Deposition. *Nature* **2013**, *501* (7467), 395–398.

(3) Kim, H. S.; Lee, C. R.; Im, J. H.; Lee, K. B.; Moehl, T.; Marchioro, A.; Moon, S. J.; Humphry-Baker, R.; Yum, J. H.; Moser, J. E.; et al. Lead Iodide Perovskite

Sensitized All-Solid-State Submicron Thin Film Mesoscopic Solar Cell with Efficiency Exceeding 9%. *Sci. Rep.* **2012**, *2*, 1–7.

(4) Yin, W.-J.; Shi, T.; Yan, Y. Unique Properties of Halide Perovskites as Possible Origins of the Superior Solar Cell Performance. *Adv. Mater.* **2014**, *26* (27), 4653–4658.

(5) Park, N.-G.; Grätzel, M.; Miyasaka, T.; Zhu, K.; Emery, K. Towards Stable and Commercially Available Perovskite Solar Cells. *Nat. Energy* **2016**, *1* (11), 16152.

(6) Zhang, W.; Eperon, G. E.; Snaith, H. J. Metal Halide Perovskites for Energy Applications. *Nat. Energy* **2016**, *1* (6), 16048.

(7) Akkerman, Q. A.; Rainò, G.; Kovalenko, M. V.; Manna, L. Genesis, Challenges and Opportunities for Colloidal Lead Halide Perovskite Nanocrystals. *Nat. Mater.* **2018**, *17* (5), 394–405.

(8) Liao, Y.; Liu, H.; Zhou, W.; Yang, D.; Shang, Y.; Shi, Z.; Li, B.; Jiang, X.; Zhang, L.; Quan, L. N.; et al. Highly Oriented Low-Dimensional Tin Halide Perovskites with Enhanced Stability and Photovoltaic Performance. *J. Am. Chem. Soc.* **2017**, *139* (19), 6693–6699.

(9) Ortiz-Cervantes, C.; Carmona-Monroy, P.; Solis-Ibarra, D. Two-Dimensional Halide Perovskites in Solar Cells: 2D or Not 2D? *ChemSusChem* **2019**, *12* (8), 1560–1575.

(10) Etgar, L. The Merit of Perovskite's Dimensionality; Can This Replace the 3D Halide Perovskite? *Energy Environ. Sci.* **2018**, *11* (2), 234–242.

(11) Chen, S.; Shi, G. Two-Dimensional Materials for Halide Perovskite-Based Optoelectronic Devices. *Advanced Materials*. 2017.

(12) Quan, L. N.; Yuan, M.; Comin, R.; Voznyy, O.; Beauregard, E. M.; Hoogland, S.; Buin, A.; Kirmani, A. R.; Zhao, K.; Amassian, A.; et al. Ligand-Stabilized Reduced-Dimensionality Perovskites. *J. Am. Chem. Soc.* **2016**, *138* (8), 2649–2655.

(13) Kendall, K. R.; Navas, C.; Thomas, J. K.; zur Loye, H.-C. Recent Developments in Oxide Ion Conductors: Aurivillius Phases. *Chem. Mater.* **1996**, *8* (3), 642–649.

(14) JARDIEL, T.; CABALLERO, A. C.; VILLEGAS, M. Aurivillius Ceramics: Bi4Ti3O12-Based Piezoelectrics. *J. Ceram. Soc. Japan* **2008**, *116* (1352), 511–518.

(15) Giannozzi, P.; Andreussi, O.; Brumme, T.; Bunau, O.; Buongiorno Nardelli, M.; Calandra, M.; Car, R.; Cavazzoni, C.; Ceresoli, D.; Cococcioni, M.; et al. Advanced Capabilities for Materials Modelling with Quantum ESPRESSO. *J. Phys. Condens. Matter* **2017**, *29* (46), 465901.

(16) Giannozzi, P.; Baroni, S.; Bonini, N.; Calandra, M.; Car, R.; Cavazzoni, C.; Ceresoli, D.; Chiarotti, G. L.; Cococcioni, M.; Dabo, I.; et al. QUANTUM ESPRESSO: A Modular and Open-Source Software Project for Quantum Simulations of Materials. *J. Phys. Condens. Matter* **2009**, *21* (39), 395502.

(17) Blöchl, P. E. Projector Augmented-Wave Method. *Phys. Rev. B - Condens. Matter Mater. Phys.* **1994**, *50* (24), 17953–17979.

(18) Perdew, J. P.; Burke, K.; Ernzerhof, M. Generalized Gradient Approximation Made Simple. *Phys. Rev. Lett.* **1996**, *77* (18), 3865–3868.

(19) Monkhorst, H.; Pack, J. Special Points for Brillouin Zone Integrations. *Phys. Rev. B* **1976**, *13* (12), 5188–5192.

(20) Li, J.; Yu, Q.; He, Y.; Stoumpos, C. C.; Niu, G.; Trimarchi, G. G.; Guo, H.; Dong, G.; Wang, D.; Wang, L.; et al. Cs 2 PbI 2 Cl 2 , All-Inorganic Two-Dimensional Ruddlesden–Popper Mixed Halide Perovskite with Optoelectronic Response. *J. Am. Chem. Soc.* **2018**, *140* (35), 11085–11090.

(21) Sutton, R. J.; Filip, M. R.; Haghighirad, A. A.; Sakai, N.; Wenger, B.; Giustino, F.; Snaith, H. J. Cubic or Orthorhombic? Revealing the Crystal Structure of Metastable Black-Phase CsPbI 3 by Theory and Experiment. *ACS Energy Lett.* **2018**, *3* (8), 1787–1794.

(22) Xiao, Z.; Meng, W.; Wang, J.; Mitzi, D. B.; Yan, Y. Searching for Promising New Perovskite-Based Photovoltaic Absorbers: The Importance of Electronic Dimensionality. *Mater. Horizons* **2017**, *4* (2), 206–216.

(23) Even, J.; Pedesseau, L.; Jancu, J. M.; Katan, C. Importance of Spin-Orbit Coupling in Hybrid Organic/Inorganic Perovskites for Photovoltaic Applications.

J. Phys. Chem. Lett. **2013**, *4* (17), 2999–3005.

(24) Sun, Y. Y.; Agiorgousis, M. L.; Zhang, P.; Zhang, S. Chalcogenide Perovskites for Photovoltaics. *Nano Lett.* **2015**, *15* (1), 581–585.

(25) Zhao, X. G.; Yang, D.; Ren, J. C.; Sun, Y.; Xiao, Z.; Zhang, L. Rational Design of Halide Double Perovskites for Optoelectronic Applications. *Joule* **2018**, *2* (9), 1662–1673.

(26) Zhao, X.-G.; Yang, D.; Sun, Y.; Li, T.; Zhang, L.; Yu, L.; Zunger, A. Cu–In Halide Perovskite Solar Absorbers. *J. Am. Chem. Soc.* **2017**, *139* (19), 6718–6725.

(27) Xiao, Z.; Yan, Y. Progress in Theoretical Study of Metal Halide Perovskite Solar Cell Materials. *Adv. Energy Mater.* **2017**, *7* (22), 1701136.

(28) Maughan, A. E.; Ganose, A. M.; Bordelon, M. M.; Miller, E. M.; Scanlon, D. O.; Neilson, J. R. Defect Tolerance to Intolerance in the Vacancy-Ordered Double Perovskite Semiconductors Cs2SnI6 and Cs2TeI6. *J. Am. Chem. Soc.* **2016**, *138* (27), 8453–8464.

(29) Slavney, A. H.; Hu, T.; Lindenberg, A. M.; Karunadasa, H. I. A Bismuth-Halide Double Perovskite with Long Carrier Recombination Lifetime for Photovoltaic Applications. *J. Am. Chem. Soc.* **2016**, *138* (7), 2138–2141.

(30) Park, B. W.; Philippe, B.; Zhang, X.; Rensmo, H.; Boschloo, G.; Johansson, E. M. J. Bismuth Based Hybrid Perovskites A3Bi2I9 (A: Methylammonium or Cesium) for Solar Cell Application. *Adv. Mater.* **2015**, *27* (43), 6806–6813.

(31) Zhao, S.; Yamamoto, K.; Iikubo, S.; Hayase, S.; Ma, T. First-Principles Study of Electronic and Optical Properties of Lead-Free Double Perovskites Cs2NaBX6 (B = Sb, Bi; X = Cl, Br, I). *J. Phys. Chem. Solids* **2018**, *117* (August 2017), 117–121.

(32) Brandt, R. E.; Kurchin, R. C.; Hoye, R. L. Z.; Poindexter, J. R.; Wilson, M. W. B.; Sulekar, S.; Lenahan, F.; Yen, P. X. T.; Stevanović, V.; Nino, J. C.; et al. Investigation of Bismuth Triiodide (BiI3) for Photovoltaic Applications. *J. Phys. Chem. Lett.* **2015**, *6* (21), 4297–4302.

(33) Hoye, R. L. Z.; Brandt, R. E.; Osherov, A.; Stevanović, V.; Stranks, S. D.; Wilson, M. W. B.; Kim, H.; Akey, A. J.; Perkins, J. D.; Kurchin, R. C.; et al.

Methylammonium Bismuth Iodide as a Lead-Free, Stable Hybrid Organic-Inorganic Solar Absorber. *Chem. - A Eur. J.* **2016**, *22* (8), 2605–2610.

(34) Chen, M.; Ju, M. G.; Carl, A. D.; Zong, Y.; Grimm, R. L.; Gu, J.; Zeng, X. C.; Zhou, Y.; Padture, N. P. Cesium Titanium(IV) Bromide Thin Films Based Stable Lead-Free Perovskite Solar Cells. *Joule* **2018**, *2* (3), 558–570.

(35) Ju, M. G.; Chen, M.; Zhou, Y.; Garces, H. F.; Dai, J.; Ma, L.; Padture, N. P.; Zeng, X. C. Earth-Abundant Nontoxic Titanium(IV)-Based Vacancy-Ordered Double Perovskite Halides with Tunable 1.0 to 1.8 EV Bandgaps for Photovoltaic Applications. *ACS Energy Lett.* **2018**, *3* (2), 297–304.

(36) Jana, M. K.; Janke, S. M.; Dirkes, D. J.; Dovletgeldi, S.; Liu, C.; Qin, X.; Gundogdu, K.; You, W.; Blum, V.; Mitzi, D. B. Direct-Bandgap 2D Silver–Bismuth Iodide Double Perovskite: The Structure-Directing Influence of an Oligothiophene Spacer Cation. *J. Am. Chem. Soc.* **2019**, *141* (19), 7955–7964.

(37) Connor, B. A.; Leppert, L.; Smith, M. D.; Neaton, J. B.; Karunadasa, H. I. Layered Halide Double Perovskites: Dimensional Reduction of Cs 2 AgBiBr 6. *J. Am. Chem. Soc.* **2018**, *140* (15), 5235–5240.